Ceramics-Silikáty 70 (1), 12-24 (2026)
www.ceramics-silikaty.cz doi: 10.13168/cs.2025.0047

SYNTHESIS–STRUCTURE–PROPERTY CORRELATION IN HYDROXYAPATITE: EFFECT OF POLYETHYLENE GLYCOL, PH, AND PHOSPHATE ADDITION DYNAMICS

#AHMAD FADLI*, DIMAS PRAMITA NUGRAHA**, FEBLIL HUDA***, AGUNG PRABOWO****, CORY DIAN ALFARISI*, RETWI RESTYANDA*, ANA ISNANI*

*Chemical Engineering Department, Engineering Faculty, Universitas Riau, Pekanbaru, 28293, Riau, Indonesia.
**Pharmacology Department, Faculty of Medical, Universitas Riau, Riau, Indonesia
***Mechanical Engineering Department, Engineering Faculty, Universitas Riau, Pekanbaru, 28293, Riau, Indonesia.
****Chemical Engineering Department, Politeknik Negeri Samarinda, Samarinda, 75131, East Kalimantan, Indonesia

#E-mail: fadliunri@yahoo.com

Submitted September 12, 2025, accepted October 21, 2026

Keywords: Hydroxyapatite, Precipitation, Polyethylene glycol, Surface area, Syringe-assisted feeding

Hydroxyapatite (HA) is a bioceramic of considerable interest in orthopaedic and dental applications due to its compositional similarity to natural bone and teeth. However, achieving the precise control over its crystallinity and surface area remains a challenge for enhancing the bioactivity and clinical performance. In this study, HA was synthesised via controlled precipitation by titrating $(NH_4)_2HPO_4$ into $Ca(NO_3)_2$ with syringe-assisted feeding, followed by calcination at 600 °C for 5 h. The influence of the polyethylene glycol (PEG), pH adjustment, phosphate feed rate, and syringe needle size was systematically examined. Among these parameters, the phosphate feed rate was identified as the most critical factor affecting both the crystallite size and specific surface area. A feed rate of 1 mL/min produced the highest surface area (45.55 $m^2 \cdot g^{-1}$), compared to 37.85 $m^2 \cdot g^{-1}$ at 3 $mL \cdot min^{-1}$, while also maintaining favourable alkaline conditions for HA nucleation and growth. These findings demonstrate that the careful regulation of feed parameters enables the reproducible tailoring of HA structural features without complex synthesis routes. The approach provides a simple and scalable pathway for producing high-surface-area HA, offering new opportunities for the development of advanced biomaterials for medical and dental applications.

INTRODUCTION

Hydroxyapatite (HAp; $Ca_{10}(PO_4)_6(OH)_2$) is a calcium phosphate ceramic that has garnered significant attention in biomedical applications due to its close resemblance to the mineral constituents of bone and teeth. This similarity confers exceptional biocompatibility, osteoconductivity, and bioactivity, making HAp an ideal material for various applications including bone grafts, dental implants, and tissue scaffolds [1, 2]. The ability of HAp to serve as a substrate for cell culture is particularly noteworthy, as microcarriers fabricated from this material have been shown to enhance the production of biological therapeutics, such as vaccines, through improved cell attachment and proliferation [3]. The physicochemical properties of hydroxyapatite, particularly the surface area and porosity, play a crucial role in its effectiveness across biomedical and biotechnological contexts. Materials with increased surface areas tend to exhibit superior bioactivity, improved ion exchange capabilities, and enhanced potential for surface modifications, which can significantly benefit applications involving bone regeneration and drug delivery systems [4, 5]. Notably, the microstructural characteristics of hydroxyapatite, including the porosity and crystalline structure, are paramount; the higher porosity often correlates with improved biological performance, but may compromise the mechanical integrity [6].

There are several methods to synthesise hydroxyapatite with specific structural characteristics. Techniques, such as sol-gel processing, hydrothermal treatments, and precipitation, are commonly used, with the precipitation method standing out due to its ease of use and environmental benefits [7, 8]. This method allows for tailored adjustments to the parameters such as the pH and reagent concentrations, which can directly influence the resulting Hap's characteristics, including the surface area and crystallinity. Specifically, the controlled addition rates of the phosphate solution during synthesis are critical; a slower addition generally yields larger, more ordered crystallites, while faster rates can lead to a higher number of smaller particles, potentially affecting the overall product quality [9].

Moreover, the choice of raw materials for the HAp synthesis has become increasingly important, especially given the shift towards sustainable practices. Natural

sources such as eggshells, which are rich in calcium carbonate, have gained attention as viable precursors for hydroxyapatite production [8, 10]. The exploitation of such sustainable resources not only provides cost-effective solutions, but also addresses environmental concerns associated with raw material extraction. The combination of natural precursors with additives, such as polyethylene glycol (PEG), can further enhance the properties of the resultant hydroxyapatite by improving the texture and surface area through templating and stabilisation [11]. Controlled synthesis conditions, particularly those involving the pH and flow rate of phosphoric acid in calcium solutions, can also dictate the nucleation and growth processes of HAp. A system employing syringe pumps has shown promise in maintaining optimal conditions for synthesis [12]. This meticulous attention to detail in the synthesis process, alongside empirical optimisation, can yield hydroxyapatite variants with desirable properties for specific applications. By correlating the synthesis parameters with the material properties, this work aims to provide new insights into the rational design of hydroxyapatite with enhanced bioactive performance. The findings are expected to contribute not only to the scientific understanding of precipitation-based synthesis, but also to practical applications, offering a simple, cost-effective, and environmentally sustainable strategy for producing hydroxyapatite suitable for advanced biomedical and biotechnological uses.

EXPERIMENTAL

Methodology

This study was designed to investigate the influence of several synthesis parameters, including the polyethylene glycol (PEG) volume, solution pH, needle size, and phosphate addition rate, on the physicochemical properties of hydroxyapatite. The experimental procedure consisted of two main stages: the synthesis of hydroxyapatite via precipitation and the subsequent characterisation of the obtained materials.

Synthesis of hydroxyapatite

A calcium nitrate $Ca(NO_3)_2$ solution (100 mL) was prepared and transferred into a glass beaker. A solution of diammonium hydrogen phosphate $(NH_4)_2HPO_4$ was then titrated dropwise into the calcium solution using a syringe under continuous stirring at 500 rpm and 60 °C until the phosphate precursor was completely added. Stirring continued for 30 min at ambient temperature in the presence of polyethylene glycol (PEG), which was introduced in volumes ranging from 0.5 to 1.5 mL. The pH of the reaction medium varied between 8 and 12 to evaluate its effect on the precipitation process.

The synthesis was further optimised by controlling the addition rate of the phosphate solution at 1, 2, and 3 $mL \cdot min^{-1}$, and by employing syringe needles of different diameters (0.8 × 38 mm, 0.9 × 38 mm, and 1.2 × 38 mm). Following precipitation, the suspension was aged at room temperature for 24 h. The resulting precipitate was separated by vacuum filtration using Whatman No. 42 filter paper and thoroughly washed with distilled water until a neutral pH was obtained. The collected solid was dried in an oven at 110 °C for 5 h and subsequently calcined in a muffle furnace at 600 °C for 5 h to enhance the crystallinity and obtain a phase-pure calcium phosphate.

Characterisation

The specific surface area and pore size distribution of the synthesised hydroxyapatite were determined by a nitrogen adsorption–desorption analysis using the Brunauer–Emmett–Teller (BET) method with a Quantachrome NOVAtouch 4LX analyser. The surface morphology and elemental composition were examined using scanning electron microscopy coupled with energy-dispersive X-ray spectroscopy (SEM–EDX, JSM-6510LA). A phase identification and crystallographic analysis were conducted by X-ray diffraction (XRD) using a MiniFlex D teX Ultra 2 diffractometer operated at 40 kV and 15 mA.

From the results of the XRD analysis, the crystal size of hydroxyapatite can be calculated using the Dyebe-Scherrer equation:

$$D\ (nm) = \frac{K\lambda}{\beta cos\theta}$$

Where: D = Size of the crystal diameter (nm); K = Scherrer's constant (0,9); λ = Wavelength of light used (Cu,λ = 0,15406 nm); β = Full width half maximum (FWHM); θ = diffraction angle

RESULTS AND DISCUSSIONS

Effect of the polyethylene glycol (peg) volume on the hap surface area

The BET surface area analysis of the hydroxyapatite synthesised at pH 10 with variations in the polyethylene glycol (PEG) volumes reveals that without PEG, the sample offers a surface area of 18.29 $m^2 \cdot g^{-1}$. The addition of PEG positively influences the surface area, increasing it to 19.43 $m^2 \cdot g^{-1}$ at 0.5 mL and further to 21.51 $m^2 \cdot g^{-1}$ at 1.0 mL. However, upon increasing the PEG volume to 1.5 mL, a decrease in the surface area to 17.76 $m^2 \cdot g^{-1}$ is observed, which falls below that of the control. This phenomenon indicates that PEG plays a significant role in adjusting the textural properties of hydroxyapatite, acting effectively as a soft template at moderate concentrations by coating the particles to

prevent agglomeration during the synthesis process [13]. Research indicates that upon calcination, the breakdown of PEG generates pore channels, which enhances the specific surface area and ensures a more uniform pore distribution, corroborating the observed improvements in surface area at PEG volumes of 0.5 and 1.0 mL [14]. It is, however, imperative to note that surpassing the optimal concentration of PEG leads to a reduction in the specific surface area. This decline can be explained by limitations in the diffusion within the reaction medium caused by the increased PEG viscosity, which hampers the ion mobility and disrupts the uniform growth of hydroxyapatite crystals [15]. As noted, excessive viscosity can exacerbate issues of particle aggregation and pore collapse during calcination, which ultimately diminishes the available surface area. The experimental findings suggest the existence of an optimal PEG concentration that harmonises the benefits of the templating effect with the required solution dynamics; exceeding this threshold may negate the advantageous effects [16].

The synthesis of hydroxyapatite (HAp) is notably influenced by the presence of polyethylene glycol (PEG) and the pH of the synthesis environment. As revealed in the scanning electron microscopy (SEM) micrographs, hydroxyapatite produced at a pH of 10 without PEG displays an irregular particle morphology characterised by non-uniform pore sizes and agglomerated particles. This agglomeration limits the creation of well-defined porous structures, which are critical in numerous applications such as biocompatible scaffolds in tissue engineering [17, 18]. The analysis signifies that at pH levels favourable for HAp synthesis, morphology can be heavily influenced by both the presence of additives like PEG and the thermal conditions during calcination.

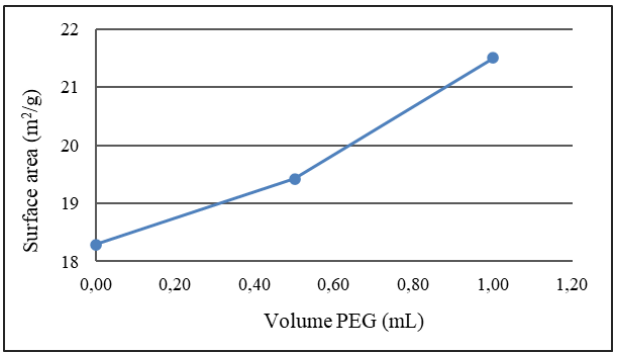

Figure 1. Curve of effect of the PEG volume on the produced surface area.

In contrast, hydroxyapatite synthesised with PEG exhibits a visibly more uniform particle morphology with larger, evenly distributed pores. Studies have shown that the templating effect of PEG contributes to the development of the interconnected porosity [18, 19]. During thermal decomposition, PEG initiates at approximately 300 °C, leading to the formation of voids as it leaves the matrix, which can be observed as pore channels within the HAp framework. The benefits of the porous morphology are evident in applications requiring high surface areas and efficient mass transport properties, particularly highlighting the use of these structures in microcarriers for bioreactors and scaffolds for tissue repair [17, 20]. The introduction of PEG significantly enhances the porosity, allowing for more advantageous physical characteristics that promote higher fluid retention and cell growth [21, 22].

The optimisation of the PEG concentration remains crucial; while moderate levels facilitate superior pore structures, excessive PEG can induce structural collapse and irregular porosity attributed to the viscosity effects during the synthesis and processing phases [23, 24]. Understanding the importance of carefully modulating PEG levels as part of the synthesis protocol is vital to

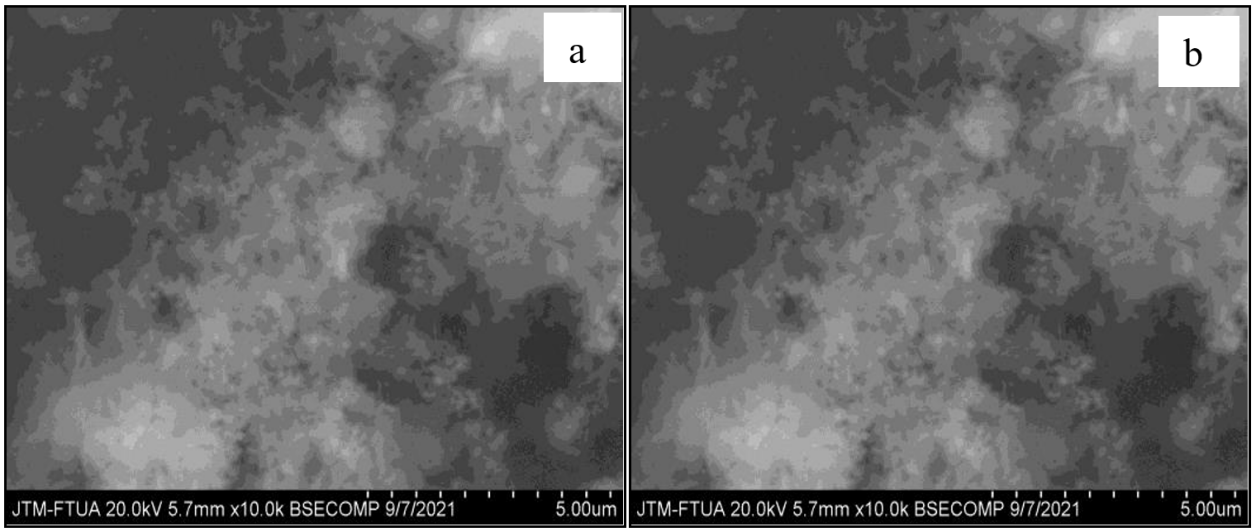

Figure 2. SEM image of hydroxyapatite (a) without PEG (b) with PEG 1 mL.

achieving a balance between maintaining the particle stability and maximising the pore development [25, 26]. Hence, the interplay of the synthesis parameters is essential in controlling the physicochemical properties of hydroxyapatite for biomedical applications.

The BJH (Barrett–Joyner–Halenda) analysis is a technique used for assessing the porosity properties of synthesised hydroxyapatite particles, specifically focusing on the pore size distribution, pore volume, and pore type. Recent studies have highlighted the significant role of polyethylene glycol (PEG) in modifying the structural characteristics of hydroxyapatite. For instance, it has been demonstrated that the incorporation of PEG leads to an increase in both the pore diameter and pore volume, thereby supporting the notion that PEG acts as a porogen during synthesis, facilitating the formation of interstitial voids [27, 28].

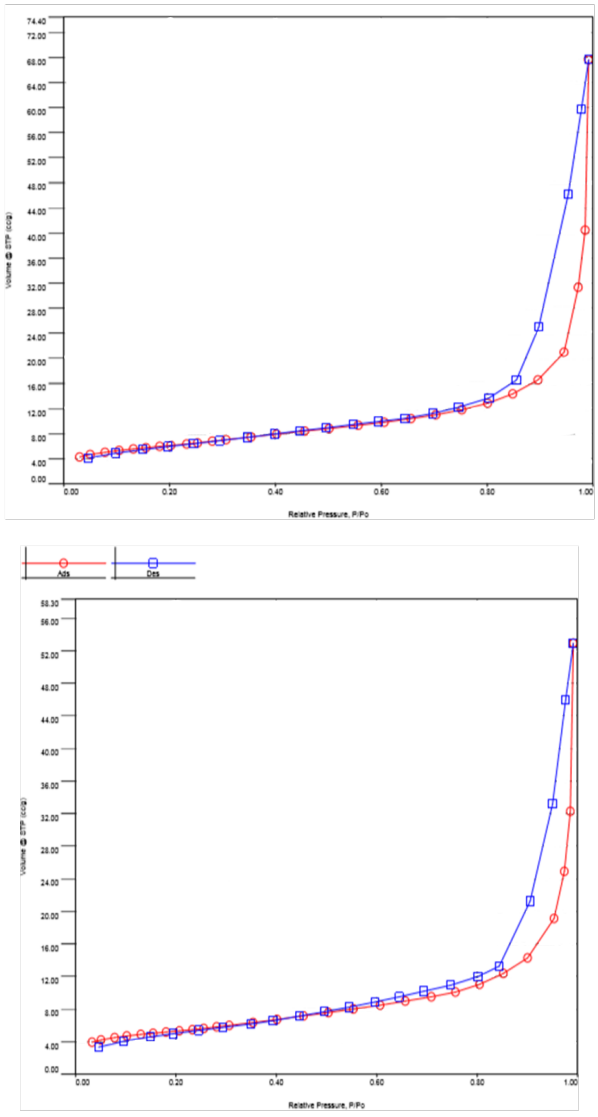

Figure 3. N_2 adsorption-desorption isotherm curve of hydroxyapatite (a) without PEG (b) with 1 mL of PEG.

The findings correspond with the International Union of Pure and Applied Chemistry (IUPAC) classification of pore sizes, wherein both PEG-modified and unmodified hydroxyapatite samples fall into the mesoporous category (2-50 nm). The non-PEG sample exhibited a pore diameter of 17.90 nm and a pore volume of 0.077 $cm^3 \cdot g^{-1}$, while the PEG-modified sample had a pore diameter of 19.45 nm and a pore volume of 0.099 $cm^3 \cdot g^{-1}$. Such enhancements in the porosity can be attributed to PEG's templating role during the calcination process, where it decomposes thermally, resulting in a more open structure that is beneficial for biomedical applications, enhancing properties essential for nutrient transport and protein adsorption [28].

This increased porosity is advantageous in biomedical applications, as it enhances a scaffold's capability for nutrient uptake and cellular interaction in tissue engineering. For example, studies have shown that the addition of organic substances like PEG, in combination with calcium phosphates, improves the material properties for bone regeneration due to their interconnected porous structures [28, 29]. Overall, improvements in the pore characteristics due to PEG incorporation align with previous research that emphasises PEG-assisted synthesis methods, demonstrating increased porosity and surface reactivity suitable for regenerative medicine applications [27, 30]

Figure 4 illustrates the X-ray diffraction (XRD) spectra of hydroxyapatite (HAp) synthesised with and without the use of polyethylene glycol (PEG). Both samples exhibit diffraction patterns indicative of crystalline hydroxyapatite, with distinct reflections that align with the standard HAp pattern (JCPDS 09-0432) [31]. The absence of additional peaks suggests that the incorporation of PEG does not introduce secondary phases such as β-tricalcium phosphate (β-TCP), calcium oxide (CaO), or amorphous calcium phosphate. This outcome is crucial because the formation of secondary calcium phosphate phases can negatively impact

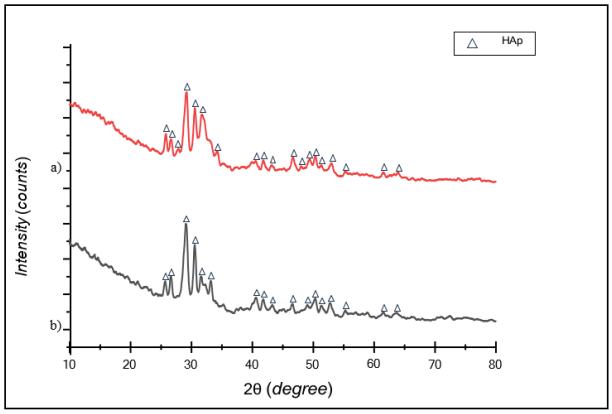

Figure 4. Diffractogram of hydroxyapatite particles a) with polyethylene glycol added b) without polyethylene glycol added.

the mechanical integrity and bioactivity in medical applications [32]. A noteworthy difference in the two spectra is the systematic shift of the diffraction peaks toward lower 2θ angles in the PEG-assisted sample compared to the control. For instance, the reflections at various angles in the PEG sample are shifted relative to their counterparts in the control sample [33]. These shifts are typically attributed to the expansion of lattice spacing resulting from lattice strain induced during the synthesis [34]. It is suggested that PEG acts as a porogenic agent, intercalating within the forming HAp matrix during the precipitation process. Upon thermal decomposition during calcination, the removal of PEG creates voids and pores, which introduce microstructural stress that leads to lattice distortion, effectively increasing the interplanar spacing and causing a shift to lower diffraction angles [35].

The calculated crystallite sizes verify this theory, demonstrating larger crystallite dimensions in the PEG-assisted HAp compared to those where PEG was not included, which is consistent with the findings that highlight PEG's ability to enhance crystallinity and promote structural order [34]. Interestingly, this scenario presents a paradox: where the lattice strain increases, crystallite size also enlarges, potentially due to the strain relaxation during calcination. As PEG burns off and pores develop, localised strain aids in merging smaller crystallites into larger grains, thereby enhancing the overall structural coherence [32]. The results revealed a significant increase in the degree of crystallinity, rising from 88.38 % in the control to 96.58 % in the PEG-assisted HAp. Higher crystallinity is vital for enhancing the physicochemical properties of hydroxyapatite, as it is linked with reduced dissolution rates, increased mechanical strength, and elevated bioactivity, particularly regarding the osteoconductivity [36]. The ability of PEG to enhance crystallinity is attributed to its templating effect during the nucleation phase, which minimises the uncontrolled agglomeration and fosters the formation of well-ordered crystal domains [37]. This is particularly significant in the context of biomedical applications, where the coexistence of high crystallinity and mesoporosity is beneficial. Conventional hydroxyapatite scaffolds often experience a trade-off between porosity and crystallinity; however, PEG-assisted synthesis allows for the generation of mesopores without compromising the crystalline order [38]. Such a combination is valuable for applications like bone tissue engineering, where high crystallinity guarantees mechanical stability and controlled resorption rates, while increased porosity enhances protein adsorption, ion exchange, and osteoblast proliferation (39 Canto, 2025).

Table 1. Crystal size of HAp made without and with the polyethylene glycol addition.

Without Polyethylene Glycol		With Polyethylene Glycol	
2θ	Crystal Size (nm)	2θ	Crystal Size (nm)
25.6205º	22.74855	25.8080º	26.55236
26.6468º	26.59766	26.6719º	26.59904
29.2136º	13.37309	29.25110	13.37423
30.5532º	26.82972	30.56800	26.83066
31.5714º	26.89602	31.65250	26.90141
33.2120º	27.00806	50.34890	2.5973

While the XRD patterns affirm the predominance of the HAp phase, it is essential to acknowledge that minor amorphous or secondary phases could remain undetected due to XRD's limitations. Additionally, the analysis of the peak broadening indicates a correlation between the micro-strain and crystallite size, suggesting that further complementary techniques, such as transmission electron microscopy (TEM) or Rietveld refinement, would yield a more precise quantification of the crystallite morphology and lattice distortion [40]. Future investigations should also delve into the effect of varying PEG molecular weights on the crystallinity and lattice strain, as the molecular characteristics of PEG can significantly influence its templating efficiency [41].

Effect of the phosphate addition rate on the hap surface area

The effect of the phosphate addition rate on the surface area of hydroxyapatite particles is presented in Figure 5. From the earlier optimisation of the porogen concentration, 1 mL of PEG was identified as the optimum amount, and this value was therefore used as the baseline for studying the phosphate addition rate at a synthesis pH of 10. This choice ensured that the influence of the phosphate delivery rate could be isolated under conditions already favourable for the mesopore formation. The results demonstrate that the specific surface area of hydroxyapatite is highly sensitive to the rate of the phosphate addition. When the phosphate solution was introduced at a rate of 1 mL·min^{-1}, the

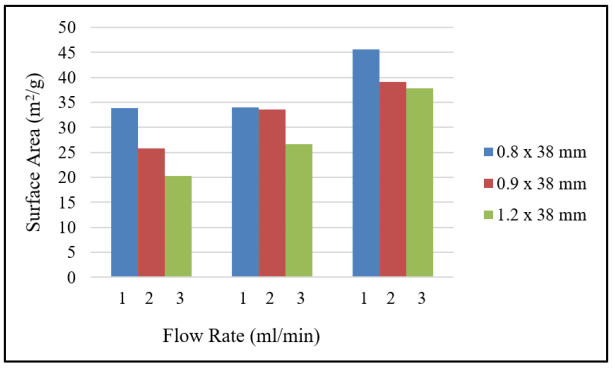

Figure 5. Effect of the needle size and phosphate addition rate on the hydroxyapatite surface area.

surface area reached 45.558 $m^2 \cdot g^{-1}$, representing the highest value among the tested conditions. By contrast, increasing the addition rate to 3 $mL \cdot min^{-1}$ resulted in a significant decrease in the surface area to 37.848 $m^2 \cdot g^{-1}$. This inverse correlation between the phosphate addition rate and surface area highlights the critical role of the reaction kinetics in controlling the textural properties of hydroxyapatite. The underlying mechanism can be explained in terms of nucleation and growth dynamics. A slower phosphate addition rate ensures gradual supersaturation, which promotes controlled nucleation followed by steady crystal growth [42].

This condition stabilises the pH within the alkaline range (pH ≈ 10), which is optimal for hydroxyapatite precipitation. Controlled nucleation minimises the particle aggregation and allows PEG to effectively act as a porogen, leading to the development of well-defined mesopores and a higher surface area. In contrast, at higher phosphate addition rates (e.g., 3 $mL \cdot min^{-1}$), the rapid influx of phosphate ions produces local supersaturation spikes. This accelerates nucleation, resulting in the formation of numerous smaller crystallites within a short time frame. While this might intuitively suggest a higher surface area, the uncontrolled nucleation simultaneously leads to greater particle aggregation and reduced porosity. Furthermore, rapid pH fluctuations destabilise the suspension, limiting the ability of PEG to uniformly template pore structures. Consequently, the resulting hydroxyapatite exhibits a lower surface area and less favourable porosity [43].

These findings align with the existing literature indicating that slower reactant feeding rates enhance the structural homogeneity and porosity during calcium phosphate synthesis. From an application perspective, tailoring the phosphate addition rate provides a straightforward approach to engineer hydroxyapatite with the desired surface properties. Materials with higher surface area and mesoporosity are particularly valuable in biomedical fields where cell adhesion, protein adsorption, and drug-loading capacity are critical. For example, hydroxyapatite microcarriers or scaffolds with higher surface area promote more efficient cell proliferation in bioreactors, while porous coatings on metallic implants enhance osseointegration by facilitating interfacial bonding with bone tissue [44, 45].

The synthesis of hydroxyapatite (HAp) particles can significantly vary based on the phosphate addition rate during the crystallisation process, influencing their morphology, distribution, and aggregation characteristics. The scanning electron microscopy (SEM) micrographs in Figure 6 taken at 40,000× magnification show that hydroxyapatite particles exhibit a characteristic rod-like morphology, linked to the preferential growth along the c-axis characteristic of hydroxyapatite crystals [46, 47, 48]. This morphology is a critical indicator of the thermodynamic stability of crystal phases, which are essential for various biomedical applications [49, 50].

When the phosphate is added at a slower rate of 1 $mL \cdot min^{-1}$, the resulting hydroxyapatite demonstrates a more uniform rod-like structure interspersed with visible pores [46, 48]. This homogenous morphology can be attributed to the controlled ion delivery that promotes gradual supersaturation, fostering orderly nucleation processes. Such conditions allow for the effective incorporation of polyethylene glycol as a pore-forming agent, producing particles with significant porosity and higher surface areas, as confirmed by the BET analysis results [51, 52]. Conversely, at a faster phosphate addition rate of 3 $mL \cdot min^{-1}$, particles are seen to be more densely packed with fewer discernible pores and irregular morphologies, suggesting that rapid ion influx disrupts controlled growth dynamics [53, 54].

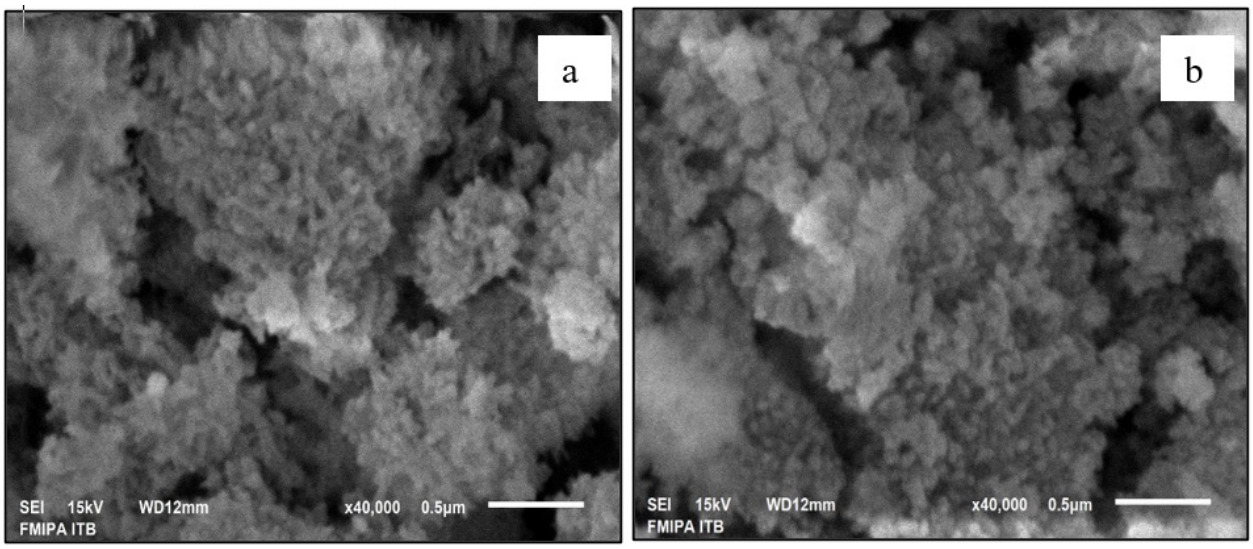

Figure 6. SEM image of the phosphate addition rate (a) 1 $ml \cdot min^{-1}$ (b) 3 $ml \cdot min^{-1}$.

This leads to accelerated nucleation and less uniform crystal growth, hence increasing the agglomeration and reducing the effective surface area, as corroborated by both the BET and BJH analyses [55, 56].

Additionally, the observation of lighter-coloured regions in the SEM images suggests the presence of agglomerated clusters, a common phenomenon in the synthesis of calcium phosphates due to the high surface energies driving the interparticle attraction, primarily mediated by van der Waals forces and hydrogen bonding [57, 58]. It has been highlighted that a slower phosphate addition can somewhat alleviate agglomeration, yielding more dispersed rod-like structures compared to denser clusters observed under higher addition rates [50, 59]. The morphological characteristics of hydroxyapatite are crucial in biomedical contexts; specifically, rod-like formations with developed porosity are particularly advantageous in bone tissue engineering, where they can facilitate protein adsorption and enhance cell attachment and nutrient diffusion, thereby improving bioactivity [51, 60].

The incorporation of secondary elements in hydroxyapatite (HAp) significantly affects its chemical stoichiometry, particularly the calcium-to-phosphorus (Ca/P) ratio, which is a widely accepted metric for assessing the quality of the material. Ideal stoichiometric HAp has a Ca/P molar ratio of approximately 1.67, similar to that found in natural bone apatite [61, 62]. However, recent analyses have indicated deviations from this ideal. For instance, studies have shown observed Ca/P ratios exceeding 1.67, raising concerns regarding the material's purity [63, 64]. This disparity typically suggests the presence of calcium-rich impurity phases such as calcium oxide (CaO), which can emerge during high-temperature processes when precursor materials do not fully decompose or are inadequately removed [65, 66]. The incomplete removal of such phases during sintering may introduce an excess of calcium relative to the phosphorus in the synthesised HAp product. The elemental composition of the synthesised HAp was characterised using an energy-dispersive X-ray (EDX) analysis, revealing primary peaks corresponding to calcium (Ca) and phosphorus (P), consistent with the expected structure of HAp. Secondary peaks from carbon (C) and oxygen (O) were also detected, indicating contributions from residual organics or ambient atmospheric influences during the analysis; the oxygen likely originates from both the phosphate framework and oxide impurities as well. The prominence of Ca and P signals in the EDX confirms that hydroxyapatite remains the predominant phase, despite the presence of minor impurities [62].

Influences on the synthesis conditions extend beyond the elemental composition; they also affect the physical properties, such as the surface area and the relative proportions of Ca and P. For instance, samples synthesised with a phosphate addition rate of 1 mL·min^{-1} exhibited higher Ca (56.92 %) and P (24.53 %) percentages compared to those produced at 3 mL·min^{-1}, which showed values of 49.57 % and 22.36 %, respectively [66, 67]. This correlation aligns with the BET results, illustrating an increased surface area at lower addition rates. Controlled phosphate delivery may enhance the efficiency of ion incorporation during crystal growth, yielding materials that are more enriched in a stoichiometric balance. The implications of deviations in the Ca/P ratio are critical when considering biomedical applications. A higher ratio often indicates calcium enrichment, which can enhance the stability and lower the solubility; however, excessive formation

Table 2. Element content of the calcium phosphate particles from the EDX analysis.

Phosphate Addition Rate (ml·min^{-1})	Element Analysis (% Massa)						
	C	O	Na	Mg	Ca	P	K
1	13.15	6.90	0.16	0.40	56.92	22.36	0.10
3	16.61	10.92	0.04	0.25	49.57	24.53	0.08

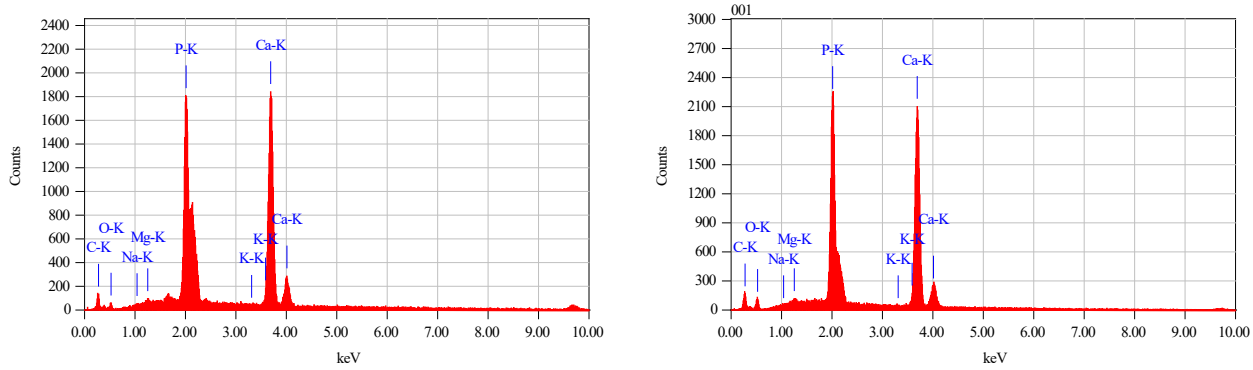

Figure 7. Energy dispersive X-ray (EDX) analysis of the phosphate addition rate (a) 1 ml·min^{-1} (b) 3 ml·min^{-1}.

of CaO may undermine the bioactivity, as CaO tends to be more basic and less biocompatible compared to pure HAp [68, 69]. Conversely, minor deviations from the stoichiometry are not uncommon within hydroxyapatite and may even confer advantageous traits, such as improved mechanical properties or altered dissolution rates, depending on the specific applications in bone tissue engineering and implant coatings [70]. Thus, the EDX findings elucidate the dual impact of varying synthesis parameters—especially the phosphate delivery rates—on the compositional and structural properties of HAp, suggesting a holistic approach to optimise the conditions for biomedical material applications.

Effect of the ph on the surface area of HAp

The influence of the pH on the textural properties of hydroxyapatite (HAp) is a critical aspect of biomaterial synthesis, particularly in the contexts of drug delivery and bone tissue engineering. An increase in the pH during synthesis significantly affects the physical characteristics of HAp, notably its surface area and pore structure. Research shows that increased pH levels, resulting in a higher hydroxide ion concentration, enhance the ionic mobility and supersaturation, leading to more frequent ionic collisions. This, in turn, accelerates the nucleation and growth of finer crystallites [71]. Studies demonstrate a marked increase in the surface area and porosity of HAp particles synthesised under alkaline conditions compared to those produced at neutral or acidic pH [72]. Table 3. Analysis result of the Brunauer Emmet Teller (BET) analysis

Table 3. Analysis result of the Brunauer Emmet Teller (BET) analysis.

pH	Surface Area ($m^2 \cdot g^{-1}$)	Pore Diameter (nm)	Pore Volume ($cm^3 \cdot g^{-1}$)
8	11.895	-	-
10	21.509	19.45	0.099
12	51.210	37.93	0.537

In experimental studies, the morphological and structural characterisation of HAp produced at various pH levels revealed crucial insights into its pore structural characteristics via the Brunauer-Emmett-Teller (BET) surface area and Barrett-Joyner-Halenda (BJH) analyses. Specifically, at pH 10, the pore diameter was recorded at approximately 19.45 nm, with a pore volume of 0.099 $cm^3 \cdot g^{-1}$; contrastingly, at pH 12, the pore diameter expanded to 37.93 nm and pore volume increased significantly to 0.537 $cm^3 \cdot g^{-1}$ [71]. This transition indicates pronounced mesoporosity arising from increased ion mobility, promoting particle aggregation and the subsequent development of larger mesopores during calcination [73]. Additionally, the adsorption-desorption isotherms associated with the synthesised HAp display type IV characteristics with H3 hysteresis loops, signifying the presence of mesoporous structures formed by plate-like aggregates. This observation correlates with the scanning electron microscopy (SEM) analyses illustrating rod-like and plate-like morphologies contributing to the overall porous architecture [72]. Such structural modifications induced by pH manipulation not only enhance the surface area, but also facilitate the engineering of hydroxyapatite with multifunctional properties crucial for biomedical applications, such as efficient drug delivery systems and scaffold designs for tissue engineering [17].

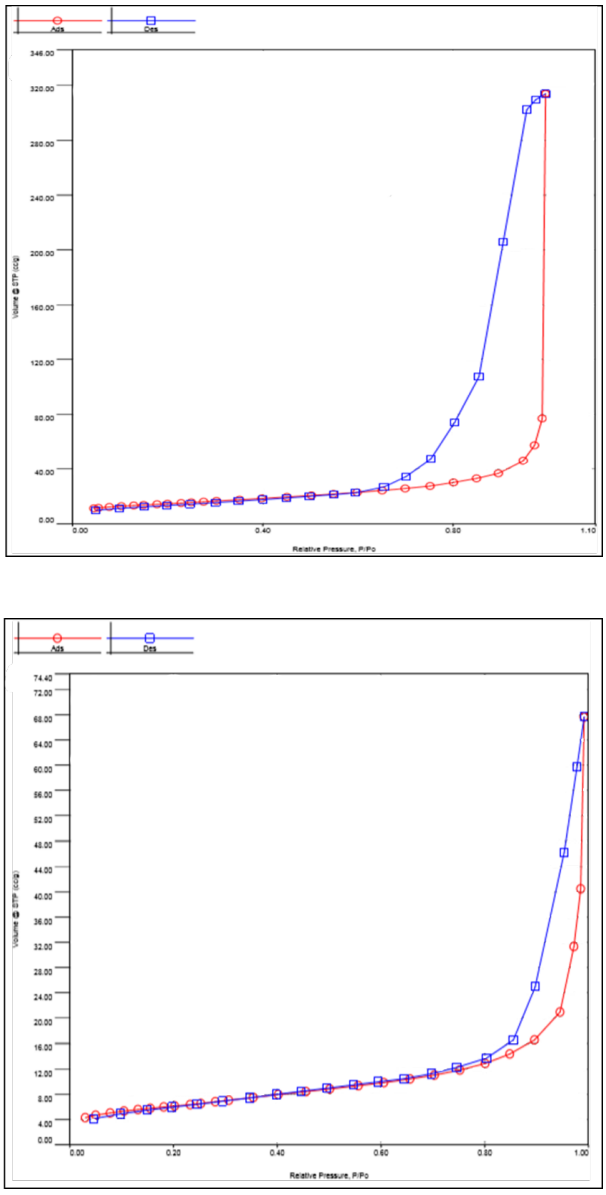

Figure 8. Adsorption-desorption isotherm curve of hydroxyapatite (a) pH 10 (b) pH 12.

The implications of these findings extend to practical applications, underscoring the importance of the pH as a controllable parameter during HAp synthesis. The balance between mechanical stability and bioactivity can be finely tuned through the pH adjustment, allowing researchers to create biomaterials that meet specific requirements for varied applications in regenerative medicine. Overall, understanding the influence of the pH on the synthesis of hydroxyapatite not only enhances material performance, but also broadens the scope of its applicability in biomedicine.

Effect of the needle size on the hap surface area

The relationship between the needle size and the synthesis of hydroxyapatite nanoparticles dramatically illustrates how crucial the experimental parameters affect the material properties such as the surface area and pH stability. In synthesising hydroxyapatite (HAp), the needle size plays an essential role in controlling the droplet dynamics, which, in turn, regulates pH levels in the reaction solution. Smaller needle sizes can lead to fluctuations in the pH, resulting in inconsistent crystal growth and potentially contributing to a diminished surface area. For instance, synthesising hydroxyapatite using a needle size of 0.8 × 38 mm resulted in a surface area of 33.891 $m^2 \cdot g^{-1}$, with pH instability reported within certain ranges. In contrast, larger needles, such as 1.2 × 38 mm, generally allow for a more stable pH and significantly increased the resulting surface area to levels noted in similar studies [74, 75].

The importance of the pH stability in mineral nucleation and crystallisation cannot be overstated. Hydroxyapatite formation is sensitive to shifts in the pH, as these changes can lead to heterogeneous nucleation events, complicating more uniform crystal growth [74, 76]. This has implications not only for laboratory-scale synthesis, but also for scale-up in industrial applications, where consistent properties are essential for biomedical uses, such as bone grafts and implant coatings [75]. For instance, studies have shown that methods like the sol-gel synthesis allow for adjustments in the pH that can refine hydroxyapatite particle characteristics, influencing their morphology and surface area [76]. Furthermore, the electrostatic effects influenced by pH can enhance the droplet stability and improve the delivery of phosphate to the growing structures. This reflects the notion that the droplet size, affected by the chosen needle diameter, significantly dictates the resulting hydroxyapatite morphology. Controlled synthesis environments have been shown to significantly affect hydroxyapatite characteristics, allowing for the production of materials with high surface areas suited for biomedical applications [77]. These materials can be particularly advantageous given their enhanced capabilities for protein adsorption and cell adhesion, essential properties for efficient tissue engineering [47, 78].

Based on Figure 9, it shows that the X-ray diffraction patterns of hydroxyapatite synthesised with different needle diameters and phosphate addition rates have the same diffraction pattern, but the diffraction peak with the same pattern shifts to the right (the angle will be smaller). This shift occurs due to the stretching of the hydroxyapatite crystal lattice so as to increase the distance between the lattice.

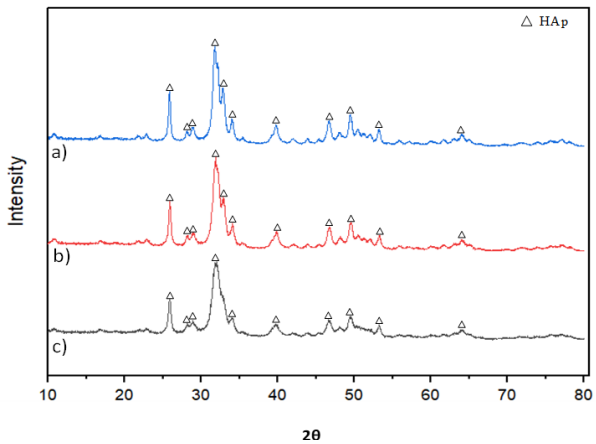

Figure 9. Diffractogram of hydroxyapatite particles a) 1.2 × 38 with a 3 $ml \cdot min^{-1}$ addition rate b) 1.2 × 38 with a 1$ml \cdot min^{-1}$ addition rate c) 0.8 × 38 with a 1 $ml \cdot min^{-1}$ addition rate.

Table 4. HAp crystal size at different needle sizes and addition rates.

	Needle Size (mm)		
	0.8 × 38	1.2 × 38	
Addition Rate ($ml \cdot min^{-1}$)	1	1	3
Crystal Size (nm)	8.4929	14.0700	12.7388

Large crystals produce diffraction peaks that are close to a vertical line. While very small crystallinity produces a very wide diffraction peak. The value of the degree of crystallinity of hydroxyapatite produced from hydroxyapatite samples with a needle diameter size of 0.8 × 38 mm at an addition rate of 1 $ml \cdot min^{-1}$ was 88.77 %, while at a needle diameter size of 1.2 × 38 mm at an addition rate of 1 $ml \cdot min^{-1}$ and 3 ml/min was 93.19 % and 91.31 %. The results of the degree of crystallinity show that there is still an amorphous phase in hydroxyapatite

CONCLUSIONS

This study has successfully demonstrated the influence of PEG, the pH, phosphate addition rate, and needle size on the textural and structural properties of

hydroxyapatite, further research is required to extend its biomedical relevance. In particular, future work should focus on correlating the optimised physicochemical properties with biological performance, including protein adsorption, cell attachment, and proliferation assays in vitro. Establishing a direct link between the synthesis parameters, surface functionality, and biological outcomes will provide stronger validation for clinical and industrial applications. Moreover, expanding this synthesis strategy to incorporate functional dopants, such as magnesium, zinc, or strontium, could further enhance the bioactivity and mechanical performance of hydroxyapatite, opening new opportunities for load-bearing implants and regenerative medicine. In addition, scaling up the process using continuous flow systems or automated syringe delivery could improve the reproducibility and cost-efficiency, making this approach more attractive for the large-scale production of medical-grade HAp. By integrating material optimisation with a biological evaluation and process scalability, future studies can advance the development of hydroxyapatite as a versatile and high-performance biomaterial for next-generation biomedical applications.

Acknowledgements

The authors are grateful to the Higher Education, Science and Technology Ministry of the Indonesian Republic for the financial support under Universitas Riau Contract No 19493/UN19.5.1.3/AL.04/2025.

REFERENCES

1. Dorozhkin S. (2022): Calcium orthophosphate (capo4)-based bioceramics: preparation, properties, and applications. *Coatings*, 12(10), 1380. doi: 10.3390/coatings12101380
2. Gunawan G., Arifin A., Yani I., Oemar B., et al. (2024): Preparation and characterization of hydroxyapatite based composite material via cold sintering process. *ARMNE*, 21(1), 127-136. doi: 10.37934/armne.21.1.127136
3. Pistone A., Iannazzo D., Celesti C., Scolaro C., et al. (2020): Chitosan/pamam/hydroxyapatite engineered drug release hydrogels with tunable rheological properties. *Polymers, 12*(4), 754. doi: 10.3390/polym12040754
4. Manjubala I., Akila R., Priya G., Anitha R., Madhan B., NarendraKumar U. (2021): Fabrication of biocomposite sheets from silk cocoons for tissue engineering applications. *International Journal of Nanotechnology, 18*(5/6/7/8), 561. doi: 10.1504/ijnt.2021.116174
5. Wei P., Zhou J., Xiong S., Yi F., et al. (2024): Chestnut-inspired hollow hydroxyapatite 3d printing scaffolds accelerate bone regeneration by recruiting calcium ions and regulating inflammation. *Acs Applied Materials & Interfaces, 16*(8), 9768-9786. doi: 10.1021/acsami.3c17087
6. Takeoka Y., Yurube T., Maeno K., Kanda Y., et al. (2020): Improved bone bonding of hydroxyapatite spacers with a high porosity in a quantitative computed tomography-image pixel analysis: a prospective 1-year comparative study of the consecutive cohort undergoing double-door cervical laminoplasty. *Jor Spine, 3*(1). doi: 10.1002/jsp2.1080
7. Sutiyono S., Edahwati L., Wahyudi M., Rahmah N. (2024): Optimization of nano-hydroxyapatite production from limestone with effect of gelatin concentration and ph in sol-gel synthesis. *International Journal of Eco-Innovation in Science and Engineering, 5*(2), 42-49. doi: 10.33005/ijeise.v5i2.137
8. Alvarado C., Alfaro A., Cisneros M., Alvarado-Quintana H. (2023): Preparation and characterization of hydroxyapatite obtained from bovine bones. *LACCEI, 1*(8). doi: 10.18687/laccei2023.1.1.590
9. Bemis R., Puspitasari R., Heriyanti H., Rahmi R., Priyanti G. (2023): The effect of variations of hydrothermal temperatures on ex-situ hydroxyapatite/Al_2O_3 doping process from papai shrimp (acetes erythraeus). *Al-Kimiya, 9*(2), 75-81. doi: 10.15575/ak.v9i2.20520
10. Lytkina D., Heinrich L., Churina E., Kurzina I. (2021): Biocompatible composite materials based on porous hydroxyapatite ceramics and copolymer of lactide and glycolide. *Materials, 14*(9), 2168. doi: 10.3390/ma14092168
11. Ju T., Zhao Z., Ma L., Li W., et al. (2021): Cyclic adenosine monophosphate-enhanced calvarial regeneration by bone marrow-derived mesenchymal stem cells on a hydroxyapatite/gelatin scaffold. Acs Omega, 6(21), 13684-13694. doi: 10.1021/acsomega.1c00881
12. Latocha J., Wojasiński M., Janowska O., Chojnacka U., et al. (2022): Morphology-controlled precipitation/remodeling of plate and rod-shaped hydroxyapatite nanoparticles. *Aiche Journal, 68*(12). doi: 10.1002/aic.17897
13. Cichoń E., Kosowska K., Pańtak P., Czechowska J., Zima A., Ślósarczyk A. (2024): Physicochemical properties of inorganic and hybrid hydroxyapatite-based granules modified with citric acid or polyethylene glycol. *Molecules, 29*(9), 2018. doi: 10.3390/molecules29092018
14. Gharehaghaji N., Divband B. (2022): Pegylated magnetite/hydroxyapatite: a green nanocomposite for t2-weighted mri and curcumin carrying. *Evidence-Based Complementary and Alternative Medicine,* 2022, 1-10. doi: 10.1155/2022/1337588
15. Carette X., Mincheva R., Gonon M., Raquez J. (2022): A simple approach for a peg-b-pla-compatibilized interface in pla/hap nanocomposite. from the design of the material to the improvement of thermal/mechanical properties and bioactivity. *Journal of Applied Polymer Science, 139*(41). doi: 10.1002/app.52807
16. Hussain M., Xie J., Hou Z., Shezad K., et al. (2017): Regulation of drug release by tuning surface textures of biodegradable polymer microparticles. *Acs Applied Materials & Interfaces, 9*(16), 14391-14400. doi: 10.1021/acsami.7b02002
17. Sari Y., Tsalsabila A., Mahardi B., Herbani Y. (2022): Effect of ph on hydroxyapatite formation in amino acid capped gold nanoparticles. *Key Engineering Materials, 931*, 83-90. doi: 10.4028/p-gki9d4
18. Fidan F., Aslan N., Koç M. (2023): Morpho-structural and compressive mechanical properties of graphene oxide reinforced hydroxyapatite scaffolds for bone tissue applications. *Research on Engineering Structures and Materials, 9*(2), 421-429. doi: 10.17515/resm2022.546me1008

19. Rekik S., Gassara S., Deratani A. (2023): Green fabrication of sustainable porous chitosan/kaolin composite membranes using polyethylene glycol as a porogen: membrane morphology and properties. *Membranes, 13*(4), 378. doi: 10.3390/membranes13040378
20. Wahda I., Kasim S., Natsir H., Fauziah S., et al. (2024): Synthesis and characterization of hydroxyapatite/SiO_2/gelatin composites as bone scaffold candidates. *Communications in Science and Technology, 9*(1), 16-24. doi: 10.21924/cst.9.1.2024.1350
21. Wu Y., Wang C., Li J., Li Y. (2021): Porous hydroxyapatite foams: excellent carrier of hydrated salt with adjustable pores for thermal energy storage. Industrial & Engineering *Chemistry Research, 60*(3), 1259-1265. doi: 10.1021/acs.iecr.0c05480
22. Kayani A., Raza M., Raza A., Hussain T., et al. (2021): Effect of varying amount of polyethylene glycol (peg-600) and 3-aminopropyltriethoxysilane on the properties of chitosan based reverse osmosis membranes. *International Journal of Molecular Sciences, 22*(5), 2290. doi: 10.3390/ijms22052290
23. Prasad N., Gayatri N., Sandhya B., Kalyani S., Bhargava S., Sridhar S. (2022): Hydrophilized ultrafiltration membranes synthesized from acrylic acid grafted polyethersulfone for downstream processing of therapeutic insulin and cobalamin. *Applied Biochemistry and Biotechnology, 194*(8), 3400-3418. doi: 10.1007/s12010-022-03822-x
24. Zhu C., Zhang X., Li F., Yang R., Zhao X. (2023): Effects of porogen peg and pore structure of pvdf substrates on the permeability–selectivity trade-off of tfc-nf membranes. *Industrial & Engineering Chemistry Research, 62*(21), 8385-8395. doi: 10.1021/acs.iecr.3c00542
25. Lai W., Liau W., Yang L. (2022): Preparation of porous biodegradable plla with tunable pore size through simple variation of peg/plla-blend crystallization conditions. *Polymers for Advanced Technologies, 34*(1), 398-404. doi: 10.1002/pat.5898
26. Shin J., Lee D., Kim B., Yoon J. (2020): Effect of polyethylene glycol molecular weight on cell growth behavior of polyvinyl alcohol/carboxymethyl cellulose/polyethylene glycol hydrogel. *Journal of Applied Polymer Science, 137*(48). doi: 10.1002/app.49568
27. Pokhrel S. (2018): Hydroxyapatite: preparation, properties and its biomedical applications. *Advances in Chemical Engineering and Science, 08*(04), 225-240. doi: 10.4236/aces.2018.84016
28. Zhang Y., Li J., Soleimani M., Giacomini F., Friedrich H., et al. (2021): Biodegradable elastic sponge from nanofibrous biphasic calcium phosphate ceramic as an advanced material for regenerative medicine. *Advanced Functional Materials, 31*(40): doi: 10.1002/adfm.202102911
29. Morejón L., Delgado J., Ribeiro A., Oliveira M., et al. (2019): Development, characterization and in vitro biological properties of scaffolds fabricated from calcium phosphate nanoparticles. *International Journal of Molecular Sciences, 20*(7), 1790. doi: 10.3390/ijms20071790
30. Ain Q., Zeeshan M., Khan S., Ali H. (2019): Biomimetic hydroxyapatite as potential polymeric nanocarrier for the treatment of rheumatoid arthritis. *Journal of Biomedical Materials Research Part A, 107*(12), 2595-2600. doi: 10.1002/jbm.a.36765
31. Shah A., Zahoor M., Muhammad N., Kamutzki F., Schmidt J., Görke O. (2023): Rapid wet chemical synthesis of bioactive glass with high yield by probe sonication. *Journal of Materials Chemistry B, 11*(20), 4416-4427. doi: 10.1039/d2tb02385g
32. Yang Y., Feng Y., Qu R., Li Q., et al. (2020): Synthesis of aligned porous polyethylene glycol/silk fibroin/hydroxyapatite scaffolds for osteoinduction in bone tissue engineering. *Stem Cell Research & Therapy, 11*(1). doi: 10.1186/s13287-020-02024-8
33. Alsalmah H., Rajeh A., Farea M., Nur O. (2024): Synthesis and characterization of peg/cs-agno3 polymer nanocomposites for flexible optoelectronic and energy storage applications. *Polymer Composites, 45*(6), 5164-5175. doi: 10.1002/pc.28118
34. Mazilu A., Popescu V., Saroşi C., Silaghi-Dumitrescu R., et al. (2021): Preparation and in vitro characterization of gels based on bromelain, whey and quince extract. *Gels, 7*(4), 191. doi: 10.3390/gels7040191
35. Shen C., Hsu S., Chang K., Yeh C., et al. (2021): Physical gold nanoparticle-decorated polyethylene glycol-hydroxyapatite composites guide osteogenesis and angiogenesis of mesenchymal stem cells. *Biomedicines, 9*(11), 1632. doi: 10.3390/biomedicines9111632
36. Sumathra M., Rajan M. (2019): Pulsed electrodeposition of hap/cpg-bsa/cur nanocomposite on titanium metal for potential bone regeneration. *Acs Applied Bio Materials, 2*(11), 4756-4768. doi: 10.1021/acsabm.9b00494
37. Song G., Guo X., Zong X., Du L., et al. (2019): Toxicity of functionalized multi-walled carbon nanotubes on bone mesenchymal stem cell in rats. *Dental Materials Journal, 38*(1), 127-135. doi: 10.4012/dmj.2017-313
38. Jamarun, N., Amelia, D., Septiani, U., & Sisca, V. (2023). The effect of temperature on the synthesis and characterization of hydroxyapatite-polyethylene glycol composites by in-situ process. *Hybrid Advances, 2*, 100031. doi: 10.1016/j.hybadv.2023.100031
39. Canto J. (2025): Teriparatide for guided bone regeneration in craniomaxillofacial defects: a systematic review of preclinical studies. *Current Issues in Molecular Biology, 47*(8), 582. doi: 10.3390/cimb47080582
40. Giannopoulos K., Lechtenfeld O. J., Holbrook T. R., Reemtsma T., Wagner S. (2020): Exploring the potential of laser desorption ionisation time-of-flight mass spectrometry to analyse organic capping agents on inorganic nanoparticle surfaces. *Analytical and Bioanalytical Chemistry, 412*(22), 5261-5271. doi: 10.1007/s00216-020-02740-3
41. Yenti S. R., Fadli A., Amri A., Novandri D., et al. (2023): Synthesis of hydroxyapatite powder using natural latex particles as pore-creating agent. *Materials Today: Proceedings, 87*, 278-283. doi: 10.1016/j.matpr.2023.03.282
42. Molino G., Palmieri M., Montalbano G., Fiorilli S., Vitale-Brovarone C. (2020): Biomimetic and mesoporous nano-hydroxyapatite for bone tissue application: a short review. *Biomedical Materials, 15*(2), 022001. doi: 10.1088/1748-605x/ab5f1a
43. Zhu Y., Xu L., Liu C., Zhang C., Wu N. (2018): Nucleation and growth of hydroxyapatite nanocrystals by hydrothermal method. *Aip Advances, 8*(8). doi: 10.1063/1.5034441
44. Fadli A., Helianty S., Nugraha D. P., Huda F., Andini N. P., Elvira P., Prabowo A. (2025): Optimisation of the ph and latex volume for expanded surface area of hydroxyapatite using the response surface methodology. *Ceramics–Silikáty, 69*(2), 171-180. doi: 10.13168/cs.2025.0003

45. Vallet-Regí M., Izquierdo-Barba I., & Colilla M. (2012): Structure and functionalization of mesoporous bioceramics for bone tissue regeneration and local drug delivery. *Philosophical Transactions of the Royal Society a Mathematical Physical and Engineering Sciences, 370*(1963), 1400-1421. doi: 10.1098/rsta.2011.0258
46. Feng G., Zheng E., Jiang F., Hu Z., et al. (2023): Group replacement–rearrangement-triggered linear-assembly nonaqueous precipitation synthesis of hydroxyapatite fibers. *Acs Biomaterials Science & Engineering, 9*(8), 4597-4606. doi: 10.1021/acsbiomaterials.3c00286
47. Wang W., Xue Z., Wang R., Wang X., Xu D. (2021): Molecular dynamics exploration of the growth mechanism of hydroxyapatite nanoparticles regulated by glutamic acid. *The Journal of Physical Chemistry B, 125*(19), 5078-5088. doi: 10.1021/acs.jpcb.1c02447
48. Chen Z., Wang X., Luo J., Zhang B., et al. (2022): Synthesis and characterization of rod-like amino acids/nanohydroxyapatite composites to inhibit osteosarcoma. *RSC Advances, 12*(55), 36103-36114. doi: 10.1039/d2ra03784j
49. Fadli, A., Widiyanti, P., Noviana, D. et al. (2022): Porous hydroxyapatite scaffold produced using Musa paradisiaca template and its in vitro bioactivity. *J Aust. Ceram. Soc., 58,* 357–366. doi: 10.1007/s41779-021-00677-z
50. Suchanek K., Perzanowski M., Lekki J., Strąg M., Marszałek M. (2019): Ammonium hydroxide mediated hydrothermal crystallization of hydroxyapatite coatings on titanium substrate. *Ceramics, 2*(1), 180-189. doi: 10.3390/ceramics2010016
51. Rosa A., Farias L., Dias V., Pacheco O., et al. (2022): Effect of synthesis temperature on crystallinity, morphology and cell viability of nanostructured hydroxyapatite via wet chemical precipitation method. *International Journal of Advances in Medical Biotechnology - Ijamb, 5*(1), 29-35. doi: 10.52466/ijamb.v5i1.110
52. Thomas S., Rakkesh R., Balakumar S. (2022): Influence of ph in the synthesis of calcium phosphate based nanostructures with enhanced bioactivity and pro-angiogenic properties. *Journal of Biomedical Materials Research Part B Applied Biomaterials, 111*(4), 858-871. doi: 10.1002/jbm.b.35196
53. In Y., Amornkitbamrung U., Hong M., Shin H. (2020): On the crystallization of hydroxyapatite under hydrothermal conditions: role of sebacic acid as an additive. *Acs Omega, 5*(42), 27204-27210. doi: 10.1021/acsomega.0c03297
54. Van H., Dũng N., Hai N., Thai C., et al. (2022): Effect of ph on structure and green emission of er/yb/mo tri-doped hydroxyapatite. *Vnu Journal of Science Mathematics - Physics, 38*(2). doi: 10.25073/2588-1124/vnumap.4680
55. Wang T., Lin C., Batalu D., Hu J., Lü W. (2020): Tunable microstructure and morphology of the self-assembly hydroxyapatite coatings on zk60 magnesium alloy substrates using hydrothermal methods. *Coatings, 11*(1), 8. doi: 10.3390/coatings11010008
56. György S., Károly Z., Fazekas P., Németh P., et al. (2019): Effect of the reaction temperature on the morphology of nanosized hap. *Journal of Thermal Analysis and Calorimetry, 138*(1), 145-151. doi: 10.1007/s10973-019-08255-z
57. Dalmônico G., Ihiawakrim D., Peña N., Biscaia E., et al. (2022): Live visualization of the nucleation and growth of needle-like hydroxyapatite crystals in solution by in situ tem. *Crystal Growth & Design, 22*(8), 4828-4837. doi: 10.1021/acs.cgd.2c00296
58. Mirković M., Kljajević L., Filipović S., Pavlović V., & Nenadović, S. (2020): Study of nanosized hydroxyapatite material annealing at different retention times. *Science of Sintering, 52*(4), 405-413. doi: 10.2298/sos2004405m
59. Beniash E., Stifler C., Sun C., Jung G., et al. (2019): The hidden structure of human enamel. *Nature Communications, 10*(1). doi: 10.1038/s41467-019-12185-7
60. Wu S., Hsu H., Wu W., Ho W. (2024): Enhancing bioactivity and mechanical properties of nano-hydroxyapatite derived from oyster shells through hydrothermal synthesis. *Nanomaterials, 14*(15), 1281. doi: 10.3390/nano14151281
61. Beaufils S., Rouillon T., Millet P., Bideau J., et al. (2019): Synthesis of calcium-deficient hydroxyapatite nanowires and nanotubes performed by template-assisted electrodeposition. *Materials Science and Engineering C, 98*, 333-346. doi: 10.1016/j.msec.2018.12.071
62. Agbeboh N., Oladele I., Daramola O., Adediran A., Olasukanmi O., Tanimola M. (2020): Environmentally sustainable processes for the synthesis of hydroxyapatite. *Heliyon, 6*(4), e03765. doi: 10.1016/j.heliyon.2020.e03765
63. Bighetti A., Cestari T., Santos P., Arantes R., et al. (2019): in vitroandin vivoassessment of cap materials for bone regenerative therapy. the role of multinucleated giant cells/osteoclasts in bone regeneration. *Journal of Biomedical Materials Research Part B Applied Biomaterials, 108*(1), 282-297. doi: 10.1002/jbm.b.34388
64. Hariani P., Muryati M., Said M., Salni S. (2020): Synthesis of nano-hydroxyapatite from snakehead (channa striata) fish bone and its antibacterial properties. *Key Engineering Materials, 840*, 293-299. doi: 10.4028/www.scientific.net/kem.840.293
65. Wibisono Y., Pratiwi A., Octaviani C., Fadila C., et al. (2021): Marine-derived biowaste conversion into bioceramic membrane materials: contrasting of hydroxyapatite synthesis methods. *Molecules, 26*(21), 6344. doi: 10.3390/molecules26216344
66. Dermawan S., Ismail Z., Jaffri M., Abdullah H. (2022): Effect of the calcination temperature on the properties of hydroxyapatite from black tilapia fish bone. *Journal of Physics Conference Series, 2169*(1), 012034. doi: 10.1088/1742-6596/2169/1/012034
67. Kastenholz H., Topper M., Warren W., Fischer M., Grass D. (2024): Noninvasive identification of carbon-based black pigments with pump-probe microscopy. *Science Advances, 10*(50). doi: 10.1126/sciadv.adp0005
68. Zhu H., Gómez M., Xiao J., Perale G., et al. (2020): Xenohybrid bone graft containing intrinsically disordered proteins shows enhanced in vitro bone formation. *Acs Applied Bio Materials, 3*(4), 2263-2274. doi: 10.1021/acsabm.0c00064
69. Hajimirzaee S., Chansai S., Hardacre C., Banks C., Doyle A. (2019): Effects of surfactant on morphology, chemical properties and catalytic activity of hydroxyapatite. *Journal of Solid State Chemistry, 276*, 345-351. doi: 10.1016/j.jssc.2019.05.031
70. Wright A., Earley E., Austin C., Arora M. (2023): Equine odontoclastic tooth resorption and hypercementosis (eotrh): microspatial distribution of trace elements in hypercementosis-affected and unaffected hard dental tissues. *Scientific Reports, 13*(1). doi: 10.1038/s41598-023-32016-6
71. Rodríguez-Lugo V., Karthik T., Mendoza-Anaya D., Rubio

E., et al. (2018): Wet chemical synthesis of nanocrystalline hydroxyapatite flakes: effect of ph and sintering temperature on structural and morphological properties. *Royal Society Open Science, 5*(8), 180962. doi: 10.1098/rsos.180962

72. Kangkan S., Arpornmaeklong P., Ummartyotin S. (2020): Synthesis of hydroxyapatite from cuttlebone under various ph conditions: an approach for medical materials. *Journal of Metals Materials and Minerals, 30*(2). doi: 10.55713/jmmm.v30i2.741
73. Ghajeri F., Leifer K., Larsson A., Engqvist H., Xia W. (2022): The influence of residuals combining temperature and reaction time on calcium phosphate transformation in a precipitation process. *Journal of Functional Biomaterials, 13*(1), 9. doi: 10.3390/jfb13010009
74. Kadu K., Tripathi R., Kowshik M., Ramanan S. (2022): Morphological evolution of hydroxyapatite nanoparticles, synthesized via modified sol-gel and microemulsion technique, in response to their synthesis microenvironment. *Kristall Und Technik, 57*(9). doi: 10.1002/crat.202200012
75. Ruffini A., Sprio S., Preti L., Tampieri A. (2019): Synthesis of nanostructured hydroxyapatite via controlled hydrothermal route. *Biomaterial-supported tissue reconstruction or regeneration,* 3. doi: 10.5772/intechopen.85091
76. Rojas-Trigos J., Jiménez-Flores Y., Suárez V., Suárez-Quezada M., Nogal U. (2018): Sol-gel synthesis of calcium-deficient hydroxyapatite: influence of the ph behavior during synthesis on the structural, chemical composition and physical properties. *Powder technology, 5*, 79-84.doi: 10.5772/intechopen.76531
77. Fadli A., Yenti S. R., Wisrayetti A. P., Hasibuan J., Herjan V. G., Isnani A., Restyanda R. (2023): Optimisation Of The Hydroxyapatite Surface Area Prepared Using A Porogen Rubber Suspension. *Ceramics–Silikáty, 67*(3), 371-378. doi: 10.13168/cs.2023.0037
78. Mendiratta S., Ali A., Hejazi S., Gates I. (2021): Dual stimuli-responsive pickering emulsions from novel magnetic hydroxyapatite nanoparticles and their characterization using a microfluidic platform. *Langmuir, 37*(4), 1353-1364. doi: 10.1021/acs.langmuir.0c02408